Remote Sensing of Environment 163 (2015) 165–179

Contents lists available at ScienceDirect

Remote Sensing of Environment

journal homepage: www.elsevier.com/locate/rse

Individual snag detection using neighborhood attribute filtered airborne lidar data

Brian M. Wing [a,*], Martin W. Ritchie [a], Kevin Boston [b], Warren B. Cohen [c], Michael J. Olsen [d]

[a] U.S.D.A. Forest Service, Pacific Southwest Research Station, 3644 Avtech Parkway, Redding, CA 96002, United States
[b] Department of Forest Engineering, Resources, & Management, Oregon State University, 204 Peavy Hall, Corvallis, OR 97331, United States
[c] U.S.D.A. Forest Service, Pacific Northwest Research Station, 3200 SW Jefferson Way, Corvallis, OR 97731, United States
[d] School of Civil and Construction Engineering, Oregon State University, 101 Kearney Hall, Corvallis, OR 97331, United States

ARTICLE INFO

Article history:
Received 26 March 2014
Received in revised form 6 March 2015
Accepted 19 March 2015
Available online 16 April 2015

Keywords:
Snags
Snag detection
Snag density
Airborne lidar
Neighborhood attribute lidar filtering
Lidar filtering
Forestry

ABSTRACT

The ability to estimate and monitor standing dead trees (snags) has been difficult due to their irregular and sparse distribution, often requiring intensive sampling methods to obtain statistically significant estimates. This study presents a new method for estimating and monitoring snags using neighborhood attribute filtered airborne discrete-return lidar data. The method first develops and then applies an automated filtering algorithm that utilizes three dimensional neighborhood lidar point-based intensity and density statistics to remove lidar points associated with live trees and retain lidar points associated with snags. A traditional airborne lidar individual-tree detection procedure is then applied to the snag-filtered lidar point cloud, resulting in stem map of identified snags with height estimates. The filtering algorithm was developed using training datasets comprised of four different forest types in wide range of stand conditions, and then applied to independent data to determine successful snag detection rates. Detection rates ranged from 43 to 100%, increasing as the size of snags increased. The overall detection rate for snags with DBH ≥ 25 cm was 56% (±2.9%) with low commission error rates. The method provides the ability to estimate snag density and stem map a large proportion of snags across the landscape. The resulting information can be used to analyze the spatial distribution of snags, provide a better understanding of wildlife snag use dynamics, assess achievement of stocking standard requirements, and bring more clarity to snag stocking standards.

Published by Elsevier Inc.

1. Introduction

In recent years, recognition of the essential roles standing dead trees (snags) play in forest ecosystems has increased. For wildlife, snags provide critical nest, roost, and den habitat for a myriad of vertebrate species while also providing excellent foraging resources (Bate, 1995; Harmon, 2002; Laudenslayer, 2002; Mellen et al., 2006; Rose et al., 2001). For these reasons snags have been classified as key habitat components for many threatened and forest health indicator species (Harmon, 2002). Snags are also important for nutrient cycling, long-term carbon storage, and many fungal and invertebrate life cycles are dependent on snags (Boddy, Frankland, & van West, 2008; Harmon, 2002; Jonsson, Kruys, & Ranius, 2005). Due to all these attributes, snags are often considered to be key indicators of biodiversity and forest health.

As the recognition of the importance of snags has become more apparent, numerous certification programs and forest management regulatory bodies have developed minimum snag stocking requirements to help ensure that biodiversity is maintained or restored (Pasher & King, 2009). These most often require a certain density or volume of snags to be maintained over time in order to provide continuous habitat support and ecosystem sustainability (Franklin, Berg, Thornburgh, & Tappeiner, 1997; Holloway, Caspersen, Vanderwel, & Naylor, 2007). The standards and regulations are often based on results from snag sampling studies, which estimate the size and quantity of snags from field sampling methods. One limitation associated with this method is that the distribution of snags across forest stands is often highly variable, even within stands that are similar in many other respects (Fan, Shifley, Thompson, & Larsen, 2004). Most standard sampling designs are not efficient for rare events, such as snags (Yoccoz, Nichols, & Boulinier, 2001). Thus, the ability to estimate and monitor snags has proven to be inherently difficult; requiring complex, intensive, and often expensive sampling procedures to produce estimates of sufficient precision (Bate, Garton, & Wisdom, 1999; Bull, Holthausen, & Marx, 1990; Ducey, Jordan, Gove, & Valentine, 2002; Gray, 2003; Harmon & Sexton, 1996; Kenning, Ducey, Brisette, & Gove, 2005; Krebs, 1989; Lämas & Stahl, 1998; Rose et al., 2001). This has led to the exploration of utilizing remote sensing technologies to better estimate snag densities and distributions across the landscape (Bater, Coops, Gergel, LeMay, & Collins, 2009; Bütler & Schlaepfer, 2004; Croft, Heller, & Hamilton, 1982; Martinuzzi et al., 2009).

* Corresponding author. Tel.: +1 916 710 1054; fax: +1 530 226 5091.
E-mail addresses: brianwing@fs.fed.us (B.M. Wing), mritchie@fs.fed.us (M.W. Ritchie), kevin.boston@oregonstate.edu (K. Boston), warren.cohen@oregonstate.edu (W.B. Cohen), michael.olsen@oregonstate.edu (M.J. Olsen).

http://dx.doi.org/10.1016/j.rse.2015.03.013
0034-4257/Published by Elsevier Inc.

Using remote sensing techniques to estimate the density and distribution of snags can provide a more practical, cost-effective, and reliable method (Bater et al., 2009). However, there have been few studies testing the capabilities of remote sensing to estimate snags. While some have used Landsat (Frescino, Edwards, & Moisen, 2001), most have utilized airborne multispectral imagery and have focused on stand-level disturbance events, such as insect outbreaks, disease or windfall (Guo, Kelly, Gong, & Liu, 2007; Hamilton, Megown, Ellenwood, Lachowski, & Maus, 2010; Kelly, Shaari, Guo, & Liu, 2004). Others have focused on the assessment of individual snags in a variety of forest types and conditions (Bütler & Schlaepfer, 2004; Croft et al., 1982; Haara & Nevalainen, 2002; Leckie, Jays, Gougeon, Sturrock, & Paradine, 2004; Pasher & King, 2009). Bütler and Schlaepfer (2004) achieved good results by developing a manual four-step individual-snag detection method that coupled airborne CIR photos (1:10,000) with a geographic information system (GIS). Their method produced an overall detection rate of 67% for snags ≥25 cm diameter at breast height (DBH), but also had many noted limitations; 1) most smaller snags were not detected, 2) high-levels of technology were required, including special software, and 3) accuracies were affected by factors such as aspect, surface slope, weather, and hour of flight. Their manual method, like most methods utilizing aerial imagery, also suffers from time and cost issues and is prone to operator interpretation bias and subjectivity errors (Bater et al., 2009). As a result, there has been an increased interest in augmenting techniques to estimate and detect snags using newer remote sensing technologies, such as airborne light detection and ranging (lidar), that have displayed potential in the identification of individual trees and the ability to predict live- and dead-tree attributes (Kim et al., 2009; Martinuzzi et al., 2009).

Airborne lidar is an active remote sensing technology employing an aircraft mounted laser capable of simultaneously mapping terrain and vegetation heights with sub-meter accuracy across large spatial extents (Lefsky, Cohen, Harding, & Parker, 2002). It has proven to be a very promising remote-sensing technology for increasing the accuracy and efficiency of large-scale forest inventories for a myriad of important forest inventory and wildlife habitat attributes (Maltamo, Malinen, Packalén, Suvanto, & Kangas, 2006; Martinuzzi et al., 2009; Næsset, 2002). Lidar data produce three-dimensional characterizations of objects in the form of point clouds that are defined by precise x, y and z coordinates. They also help characterize the reflectance and surface properties of intersected objects by providing intensity values, which are a measure of return-signal strength for each point. These attributes are useful for forest inventory and characterization because, in theory every object in a forest can be detected if adequate lidar point densities are collected within all vertical layers (e.g., understory & overstory) (Pesonen, Maltamo, Eerikäinen, & Packalén, 2008).

The use of airborne lidar in the estimation of snag attributes has received more attention recently. The methods for estimating snag attributes using airborne lidar can be separated into two assessment categories: plot-based and individual-tree (Reutebuch, Andersen, & McGaughey, 2005). Plot-based assessments seek to estimate plot-level attributes such as snag volume, biomass or abundance (Bater et al., 2009; Kim et al., 2009; Martinuzzi et al., 2009; Pesonen et al., 2008), while individual-tree based assessments seek to extract and measure individual trees using some type of segmentation method (Kaartinen & Hyyppä, 2008; Vauhkonen et al., 2011). Estimation of snag attributes using plot-based assessment methods have achieved mixed results. Pesonen et al. (2008) achieved relatively poor results predicting snag volume using plot-based canopy derived lidar-metrics (RMSE 79%), while Kim et al. (2009) achieved better results estimating snag biomass using similar plot-based metrics that were stratified based on intensity values. These studies both highlight the need for more research on the subject.

Individual-tree based snag assessment using airborne lidar has received less attention. All studies to date using individual-tree based assessment methods have focused on extracting both live and dead trees, with most attention on the former (Kaartinen & Hyyppä, 2008; Maltamo, Eerikäinen, Pitkänen, Hyyppä, & Vehmas, 2004; Mehtätalo, 2006; Morsdorf et al., 2010; Reitberger, Schörr, Krzystek, & Stilla, 2009; Vauhkonen et al., 2011; Wang, Weinacker, Koch, & Sterenczak, 2008). To the authors' knowledge, there have been no studies to date that have predominantly focused on identification of individual snags using an airborne lidar individual-tree assessment method. This study attempts to identify individual snags using airborne lidar data by applying an individual-tree assessment method to neighborhood attribute filtered lidar data focused on removing lidar points associated with live trees from the overstory (snag-filtered lidar data).

Neighborhood attribute point cloud filtering is a new airborne lidar analysis technique being introduced in this study. Its primary objective is to create an automated routine that accurately assigns the proper forest attribute to each lidar point. This information can then be used to filter the points and obtain a point cloud containing only points associated with the forest attribute(s) of interest, or to assign individual forest attribute probabilities or weights to each lidar point. In theory, this should provide an enhanced airborne lidar analysis framework for both plot-based and individual forest attribute assessments since lidar points not associated with the forest attribute(s) of interest are either removed from the analysis or have less influence on prediction models. Filtering is accomplished by using two inherent lidar point attributes: location and intensity. Each lidar point's attributes as well as its neighboring lidar points' attributes are used to create neighborhood statistics that are then used in a conditional framework to identify the forest attribute most likely to be associated with each lidar point. The location of each lidar point can be used to determine if a point intersected a forest attribute in the understory or overstory, and then neighborhood intensity and point density statistics can be used to help determine the unique forest attribute associated with each point. In this study, location and three dimensional (3D) neighborhood statistics are used in an attempt to identify individual lidar points associated with snags and live trees. Intensity is the primary lidar attribute used for the neighborhood point cloud filtering, therefore understanding the attribute's nuances are fundamental to successfully filtering the data.

Intensity values are an often underexploited feature of lidar data, due to variability and difficulty associated with acquisition settings and calibration (Wing et al., 2012). Intensity is a unitless measure of a laser pulse's discrete return energy stored as an integer value with a defined range (e.g., 0–255). Intensity data are primarily a measure of surface reflectance and are a function of the wavelength of the source energy, path distance, and the composition and orientation of the surface or object the laser pulse intersects (Boyd & Hill, 2007). Variability of the intensity data across similar targets is dependent upon adjustable lidar acquisition parameters. Laser beam divergence, type of source energy, path lengths and variable gain control settings all affect the variability of intensity. These acquisition parameters influence intensity at different rates and magnitudes, with path lengths and the variable gain control setting having the most influence. These attributes have limited the use of intensity data, due to variability associated with intensity values within and from different acquisitions. Even with these limitations intensity has already been used successfully in many forestry applications to differentiate between tree species, estimate live and dead biomass, and predict basal area (Donoghue, Watt, Cox, & Wilson, 2007; Holmgren & Persson, 2004; Hudak et al., 2006; Kim et al., 2009; Lim, Treitz, Baldwin, Morrison, & Green, 2003; Wing et al., 2012). Kim et al. (2009) used intensity value threshold stratification to estimate live and dead standing tree biomass. They stratified plot point clouds based on intensity values and found metrics created with the lower intensity plot point cloud better estimated standing dead biomass. More recently, Wing et al. (2012) utilized intensity information to help filter points in the understory (e.g., vegetation, stumps, coarse woody debris, tree boles). These studies point toward the potential of using intensity to help characterize many forest attributes. With the advent of post-calibration or normalization routines to reduce intensity variability and the standardization of

acquisition techniques the usefulness of intensity information is likely to increase (Wing et al., 2012).

In theory, lidar points associated with snags should have different reflectance and surface properties (intensity values) compared to live trees since they contain no photosynthetic material and often lack foliage and fine branches. If true, it might be possible to exploit this relationship to determine if an individual lidar point is associated with a live tree or snag. This study tests this theory by attempting to create an automated snag-filtering algorithm that classifies each overstory lidar point as a live tree or snag point. Lidar points classified as snag points are retained in the overstory, while live tree points are removed. After the algorithm is applied, a traditional canopy surface model individual-tree segmentation procedure is employed to identify individual snags, estimate their heights and generate a snag stem map. In summary, the objectives of this study are to 1) create a neighborhood attribute filtering algorithm that removes points associated with live trees from the overstory, 2) apply an individual-snag detection method to the snag-filtered point cloud, and 3) test the detection and error rates in various forest types and structures to help determine applicability in different forest conditions.

2. Materials and methods

2.1. Study area

The study was conducted at two sites: Blacks Mountain Experimental Forest (BMEF) and the Storrie Fire restoration area (SF). Both are located in northeastern California (Fig. 1). BMEF is managed by the USDA Forest Service Pacific Southwest Research Station and is located approximately 35 km northeast of Lassen Volcanic National Park and ranges between 1700 and 2100 m elevation (Fig. 1). Classified as an interior ponderosa pine forest type (Forest Cover Type 237) (Eyre, 1980), the 4358 ha forest has a wide range of stand conditions as a result of past research and management activities, as well as disturbance events (Ritchie, Skinner, & Hamilton, 2007).

As part of a large-scale, long-term interdisciplinary experimental design at BMEF initiated in 1991, two contrasting stand structures were created: low structural diversity (LoD) and high structural diversity (HiD) (Oliver, 2000). LoD stands were thinned to maintain a single canopy layer of intermediate trees, with the goal of simplifying forest tree structure. In contrast, the HiD units retained all canopy layers, which resulted in stands that feature multiple age classes and varying

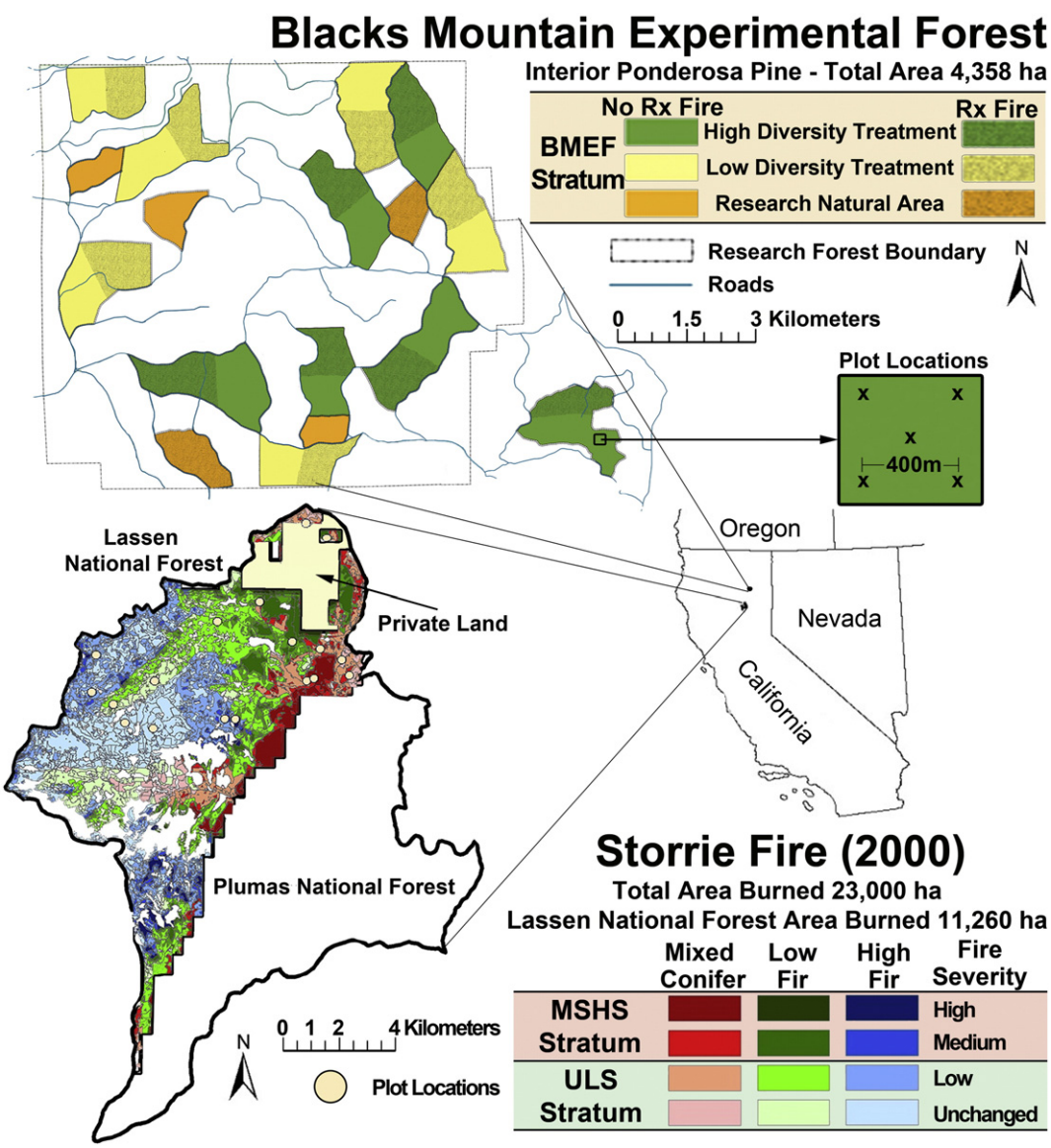

Fig. 1. Locations of Blacks Mountain Experimental Forest (BMEF) and the Storrie Fire (SF) study areas with the layout of the strata and plot locations.

crown structures (Oliver, 2000). Six research units each were randomly assigned from both the LoD and HiD treatments ranging in size from 77 to 144 ha. Each unit was then split in half with one randomly assigned half receiving prescribed fire treatments (Fig. 1). Also included at BMEF, are four research natural areas (RNA) each approximately 40 ha in size. The RNAs were set aside to serve as unmanaged, qualitative controls representative of the interior ponderosa pine forest type. They have never received mechanical treatment, but fire exclusion has greatly increased their understory tree densities. Two of the four RNAs also received one application of prescribed fire in the late 1990's.

As part of the experimental design all 16 research units at BMEF have permanent grid markers located within them utilizing a 100 × 100 m lattice pattern. The permanent grid markers serve as the center points for the plot level research being conducted on the forest. Each grid was located by conventional survey methods and placed within 15 cm of their predetermined UTM coordinates using the High Precision Geodetic Network along with survey grade GPS (Oliver, 2000).

The Storrie Fire restoration area, managed by the USDA Forest Service Lassen and Plumas National Forests (NF), is located approximately 45 km south of Lassen Volcanic National Park and ranges between 900 and 2100 m elevation (Fig. 1). The area was subject to a wildfire in late August of 2000. The fire was characterized by high spatial complexity with varying levels of fire severity on the predominantly forested landscape, burning approximately 23,000 ha (Crotteau, Varner, & Ritchie, 2012). This study only focused on the Lassen NF portion of the fire, which encompassed 48% of the area (11,260 ha). It has three dominant vegetation cover types: High Elevation Fir (HF), Low Fir (LF), and Sierra Nevada Mixed Conifer (MC) (Forest Cover Types 207, 211, and 243 respectively) (Eyre, 1980).

Variable fire severity created a mosaic of different forest conditions within each of the three forest vegetation cover types. The area was stratified into twelve total classes: four levels of fire-severity (high (HS), medium (MS), low (LS), and unchanged (U)) across three levels of forest type (HF, LF, and MC) (Fig. 1). Fire severity was determined by using the Relative differenced Normalized Burn Ratio (RdNBR; see Miller et al., 2008) to approximate the Composite Burn Index (CBI) produced from the two Landsat Thematic Mapper post-Storrie Fire images yielding the four nominal categories. The high-severity stratum can be generally characterized as having no surviving live-tree component with numerous snags at similar decay stages, which were often broken at the time of the study. The medium-severity stratum has very few live trees and numerous snags at various stages of decay. The low-severity stratum has a higher proportion of live trees with some snags at various stages of decay. The unchanged stratum generally has little or no fire-induced mortality in the overstory. Any snags within the unchanged stratum were unlikely to have been killed by the Storrie Fire.

For this study, the two study areas were grouped into three logical strata for analysis. All plots at BMEF were combined to create one stratum that represents the broad diversity of stand structures commonly found in the interior ponderosa pine forest type (Fig. 1). At SF, due to lower plot densities, the twelve stratified classes were grouped into two new strata by first combining all three forest types and then grouping the four fire severity classes into two categories. The first stratum is comprised of all U and LS plots (SF-ULS) and the second is comprised of all MS and HS plots (SF-MSHS) (Fig. 1).

2.2. Field data

At BMEF, five of the LoD units, six of the HiD units and 2 randomly selected RNAs were sampled in July 2009. Standing live (DBH ≥ 9 cm) and dead tree (DBH ≥ 12 cm) stand attributes for BMEF at the time of the study are summarized in Table 1. Using the BMEF permanent grid system, plot locations were systematically located with a random start within each unit on every other grid point in all intercardinal directions (282 m spacing). At each selected grid point, an 805 m^2 circular plot was established. All trees (live: DBH ≥ 9 cm; dead: DBH ≥ 12 cm) were stem mapped from plot center and measured for height, DBH, crown width, and height to live and dead crown. Trees were also assigned codes for various tree conditions (i.e., broken, dead or forked top, sweep or lean, mistletoe presence, epicormic branching, etc.). Trees having DBH ≥ 50 cm were also assigned vigor condition class risk ratings using the systems developed by Ferrell (1989) for non-pine species (e.g. white & red fir and incense cedar) and Salman and Bongberg (1942) for pine species. The classification systems resulted in individual tree vigor risk ratings ranging from 1 to 3 for the non-pine species and 1 to 4 for pine species, with higher risk ratings associated with declining tree vigor. All snags were given a decay condition class rating using the system developed by Thomas, Anderson, Maser, and Bull (1979).

At SF, two plot clusters were randomly located within each of the twelve original strata. Each plot cluster was comprised of three evenly spaced (50 m) circular plots (16 m-radius, 805 m^2). Plot clusters were located by first selecting a location within each stratum for the initial plot's establishment. Next, a randomly selected azimuth was used to determine the location of the two adjacent plots. All standing trees were measured in August 2009 using the same sampling protocol utilized at BMEF. Access to the SF area is limited and due to time constraints six strata only received one cluster. Plots were located and permanently established using high-grade GPS in the field. Standing live and dead tree attributes for SF at the time of the study are summarized in Table 1.

2.3. Lidar data

Discrete return airborne lidar data were acquired by Watershed Sciences Inc. (current name: Quantum Spatial Inc.) in late July 2009 using a Leica ALS50 Phase II laser system (near-infrared) mounted on a fixed wing aircraft. The aircraft was flown at 900 m above ground

Table 1
Standing live tree (DBH ≥ 9 cm) and snag (DBH ≥ 11.5 cm; heights ≥ 3 m) stand attributes from plot data for the three strata (n_t = number of snags; n_p = number of plots; SD = standard deviation).

Strata	n_t	DBH (cm)			Height (m)			n_p	Trees ha^{-1}		
		Range	Mean	SD	Range	Mean	SD		Range	Mean	SD
BMEF — live trees	3819	(9.0–135.1)	25.6	15.4	(1.8–41.4)	12.4	6.3	154	(24.7–1469.7)	306.3	238.6
Storrie (ULS) — live trees	675	(9.1–160.3)	37.0	24.4	(3.1–55.2)	17.8	10.9	30	(37.1–667.0)	260.4	153.9
Storrie (MSHS) — live trees	92	(13.2–105.7)	50.0	22.4	(4.0–44.2)	24.1	9.5	22	(0.0–94.7)	51.7	48.4
BMEF — snags (overall)	261	(11.5–122.2)	30.8	21.8	(3.0–42.7)	11.6	6.7	154	(0.0–197.6)	21.9	34.4
BMEF — snags (training)	94	(11.5–94.2)	29.3	21.4	(3.0–42.7)	12.3	7.5	36	(0.0–197.6)	46.1	48.5
BMEF — snags (independent)	167	(11.5–122.2)	32.1	22.2	(3.0–35)	11.0	6.0	118	(0.0–123.5)	15.8	24.2
Storrie (ULS) — snags (overall)	169	(11.5–137.4)	44.4	27.5	(3.0–49.7)	13.6	10.0	30	(0.0–308.8)	79.9	75.6
Storrie (ULS) — snags (training)	51	(11.5–137.4)	56.6	33.7	(3.0–49.7)	16.0	11.3	10	(37.1–172.9)	71.4	43.1
Storrie (ULS) — snags (independent)	118	(11.9–128.0)	39.5	22.9	(3.1–47.6)	12.6	9.2	20	(0.0–308.8)	76.5	73.6
Storrie (MSHS) — snags (overall)	258	(11.7–110.0)	39.4	19.0	(3.1–42.7)	10.7	7.0	22	(24.7–333.5)	149.7	93.3
Storrie (MSHS) — snags (training)	91	(11.7–110.0)	40.4	21.2	(3.0–34.7)	10.5	7.6	7	(61.75–284.1)	162.3	77.9
Storrie (MSHS) — snags (independent)	167	(12.2–87.6)	38.9	17.7	(3.1–42.7)	10.9	6.7	15	(24.7–333.5)	140.0	92.9

level following topography. Data were acquired using an opposing flight line side-lap of ≥50% and a sensor scan angle ±14° from nadir. On-ground laser beam diameter was approximately 25 cm (narrow beam divergence setting), which resulted in a very low percentage of multiple returns (BMEF: 9.2%; SF: 10.1%) and a very high percentage of single returns (BMEF: 81.4% & SF: 78.2%). At BMEF, an average of 6.9 points m^{-2} was obtained for the entire study area, with a standard deviation of 5.6 points m^{-2}. At SF, an average of 6.7 points m^{-2} was obtained for the entire study area, with a standard deviation of 5.9 points m^{-2}.

The vendor post-processed lidar data using automated methods in proprietary software (TerraScan) coupled with manual methods to identify ground points for development of the digital terrain model (DTM). Vertical DTM accuracy for both study locations was approximately 15 cm at a 95% confidence level. The vendor used an automatic variable gain setting during acquisition and did not calibrate the intensity values post-acquisition.

2.4. Data analysis

Data analysis is presented in four sections: 1) lidar data pre-processing, 2) snag-filtering algorithm, 3) individual-snag detection, and 4) snag detection and error rates. The study's overall data analysis workflow is summarized in Fig. 2 for reference.

2.4.1. Lidar data pre-processing

Inaccurate plot locations are one of largest sources of model error found in many types of airborne lidar analysis (Anderson, Clarkin, Winterberger, & Strunk, 2009; Hawbaker et al., 2009). To reduce plot location errors, all plot locations were manually corrected using the field-derived standing tree stem map and corresponding lidar data for each 809 m^2 circular plot at both BMEF and SF. Due to BMEF's highly accurate permanent grid system no plot locations needed correction; while at SF most plots needed location correction. All plot locations were found to be highly accurate after this process was completed (±1 m). Next, the lidar point cloud elevation values were normalized into height values using the lidar-derived DTM. Height normalized point clouds corresponding to the 805 m^2 circular plots with a 5 m buffer were extracted for further analysis. The 5 m plot buffer was added to each plot to eliminate edge effect issues associated with the snag-filtering algorithm, the canopy surface model creation method, and the individual-tree segmentation procedure. In the final step, the overstory minimum height thresholds were determined from field data for both study locations (BMEF: lidar height ≥ 1.5 m; SF: lidar height ≥ 2 m). After these pre-processing steps were completed the neighborhood snag-filtering algorithm was applied to the height normalized plot point clouds.

2.4.2. Snag-filtering algorithm

The goal of the automated snag-filtering algorithm is to accurately classify each overstory lidar point as live tree or snag using individual point location attributes and neighborhood intensity and point density statistics. To properly use the intensity information for this purpose, the dynamics of intensity data quality and in relation to live trees and snags must first be understood. As previously discussed, the quality of intensity information is dependent upon acquisition and calibration methods. Morsdorf et al. (2010) showed that the first and single returns provided more accurate intensity information. Therefore, only the first and single returns were used in this study. The lidar acquisition method used for both study areas resulted in first and single return intensity values ranging from 0 to 255 i (i will act as the intensity value index).

Individual tree point clouds from 40 randomly selected snags and 100 randomly selected live trees were extracted and analyzed for trends from both study locations to aid with understanding the intensity dynamics in relation to live trees and snags (Fig. 3). For the lidar datasets used in this study the following intensity trends were identified:

For snags:

1) Snags were comprised of a high proportion (~85%) of lower valued intensity points (0–60 i). These points are most likely associated with solid woody material (i.e., branches or boles).
2) Some snags contained a relatively small percentage (~10%) of points with very high intensity values (>160 i). These points are thought to be associated with bare wood that has seasoned, thus creating a light-colored, somewhat smooth reflective surface.
3) Some snags had a low percentage (~10%) of points with mid-range intensity values (60–160 i). The reason for these is uncertain, but they tended to be associated with snags that contained one or more of the following; 1) witches broom (usually formed from mistletoe), 2) sparse dead needles or leaves, or 3) recently dead trees still displaying fine branches. They might also be associated with lichen, although this was not sampled.

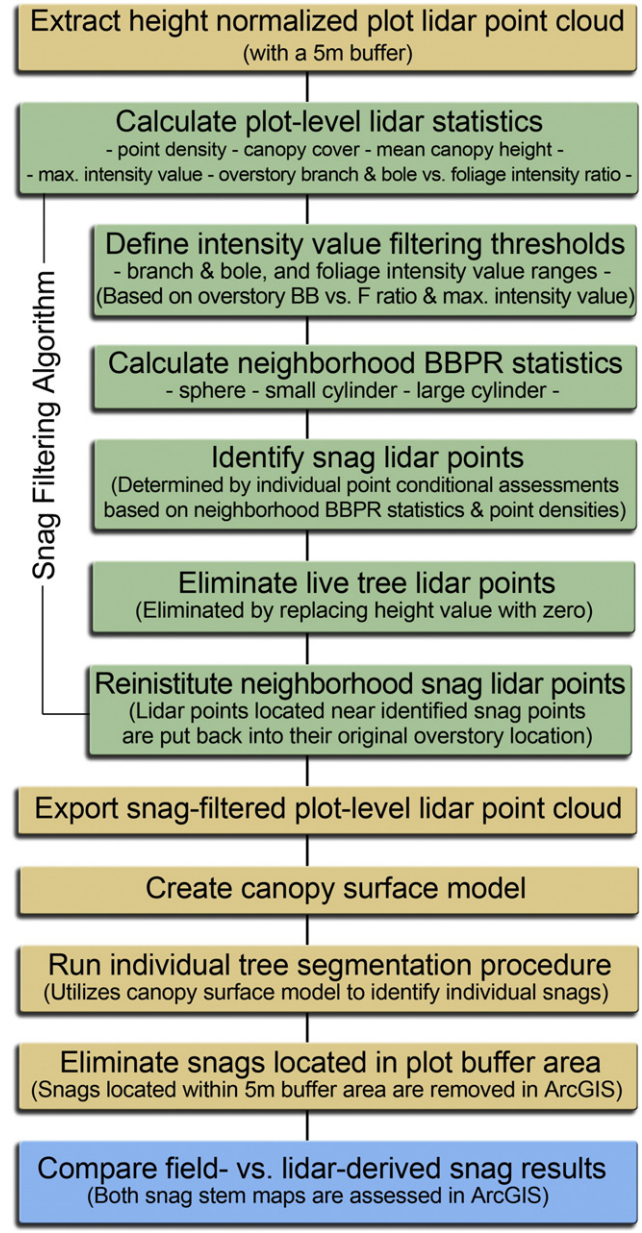

Fig. 2. Overall data analysis workflow with summarized explanations for the study.

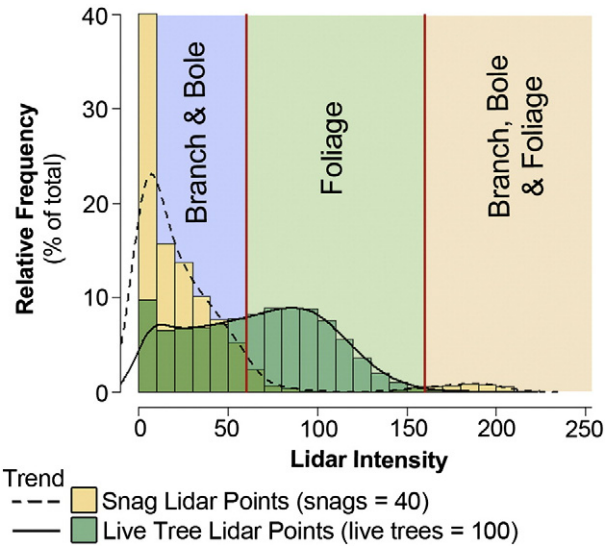

Fig. 3. Individual live tree and snag intensity histograms summarizing the intensity dynamics in relation to live trees and snags.

For live trees:

1) Live tree intensity values were typically a mix of low (0–60 i) and mid-range values (60–160 i). The low intensity values were likely associated with the tree bole and woody branches as they were most often located in the interior portion and outer crown edges of individual tree point clouds. The mid-range intensity values were most likely associated with foliage or fine branches.
2) A small percentage of points associated with live trees (~5%) displayed high intensity values (>160 i). The reason for these is uncertain, but they tended to be associated with tree tops and possibly new leader growth.

The identified live tree and snag intensity trends provided the foundation for the creation of the lidar point filtering algorithm. The filtering algorithm was developed using training datasets from all three strata (i.e., BMEF, SF-ULS, and SF-MSHS) with the intention of capitalizing on the aforementioned intensity characteristics. At BMEF, the training dataset consisted of a stratified random sample of 36 plots (3 plots from each HiD and LoD research unit with 2 of them containing at least one snag; and 3 plots from the two RNA research units with two of them containing at least one snag). At SF, the training dataset consisted of one randomly selected plot from each of the plot clusters (i.e., SF-ULS: 10 plots; SF-MSHS: 7 plots). The training datasets were combined to develop the snag-filtering algorithm. The remaining 153 plots (BMEF: 118; SF: 35) served as an independent dataset to test the methods performance.

There are four basic stages in the algorithm. In the first stage, plot-level lidar variables are calculated which are used to train the sensitivity of the algorithm. In the second stage, individual point neighborhood intensity and point density statistics are calculated for three separate 3D neighborhood variables (Fig. 4). These variables are then used in the third stage, where they are tested in a conditional assessment framework to determine whether an individual point is associated with a live tree or snag. In the fourth and final stage, all overstory points located within a 1 m radius cylinder of the snag classified points are classified as snag points. Then all points not receiving a snag classification are classified as live tree points and are eliminated by replacing their height values with a zero value to create the final snag-filtered point cloud.

2.4.2.1. Stage one — calculate plot-level lidar variables. Five plot-level lidar variables were used to train and determine the sensitivity of the algorithm's ability to identify individual snag points (Fig. 5). Each plot's

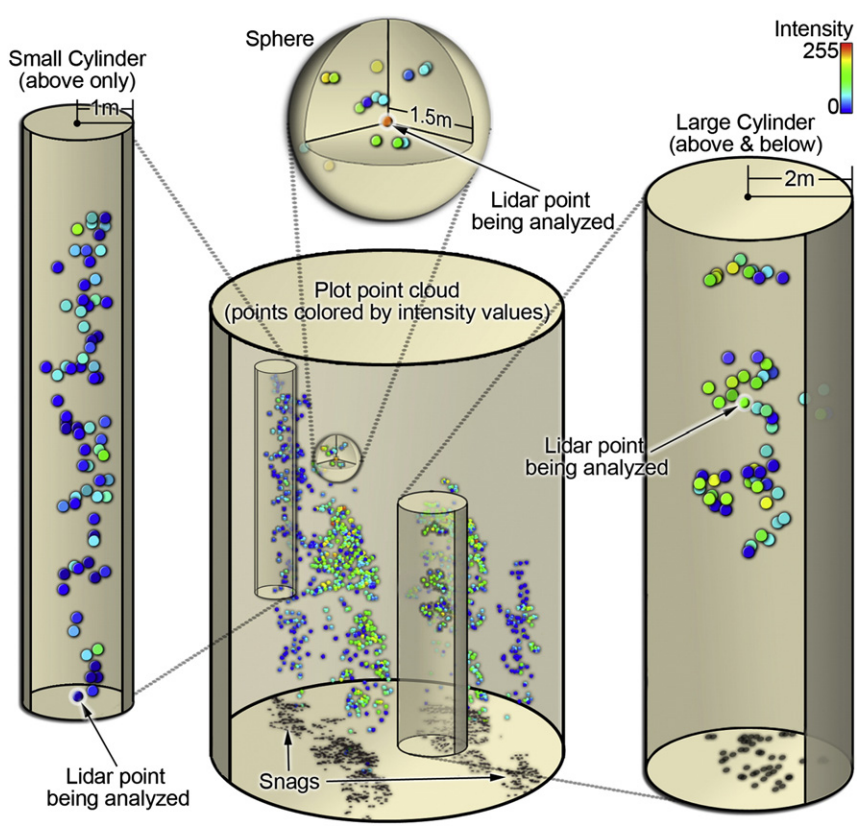

Fig. 4. Depiction of the three 3D neighborhood variables utilized in the snag-filtering algorithm. Lidar points are colored by intensity values.

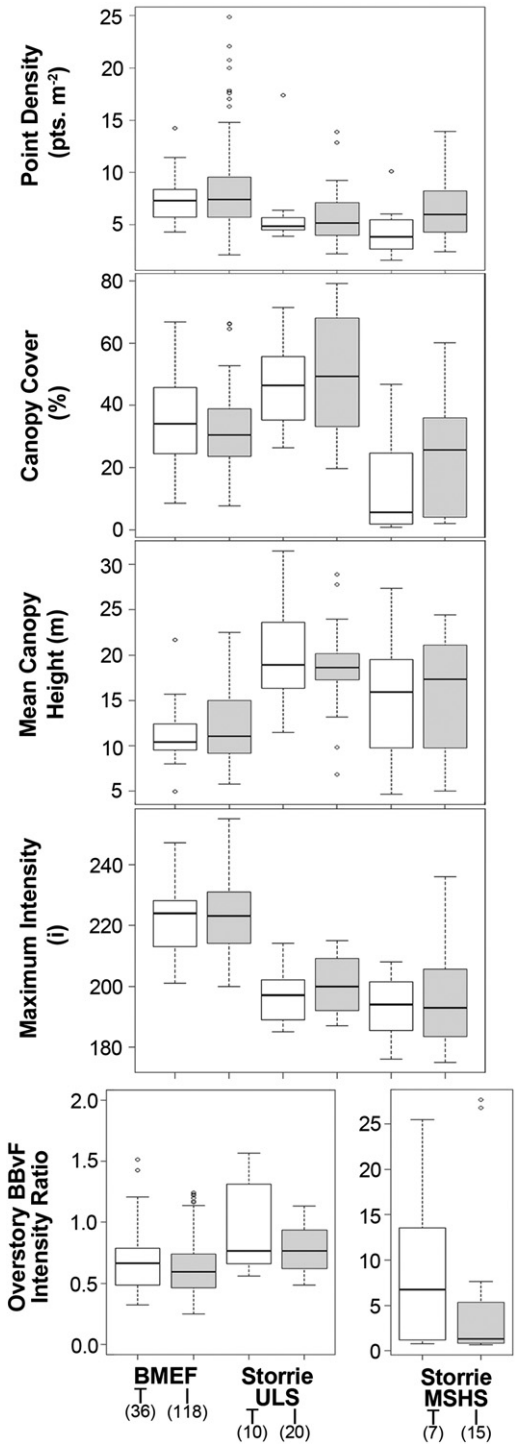

Fig. 5. Box distribution plots for the five variables used to determine the snag-filtering algorithm's sensitivity level. Box plots are given for both the training and independent datasets.

entire first and single return point cloud was used to calculate the plot's point density, maximum intensity (MaxInt), and canopy cover (i.e., total number of overstory points / total number of points); while only the overstory first and single returns were used to calculate the plot's mean canopy height (i.e., sum of overstory point heights / total number of overstory points), and the branch and bole (BB) versus foliage (F) intensity ratio (BBvFr).

BBvFr is a new overstory lidar variable that is used in two separate instances within the algorithm to help normalize local intensity variations caused by acquisition settings (e.g., gain setting variability) and local tree attributes (e.g., local tree health and vigor variability), and regulate the algorithm's sensitivity in the identification of snag points. It is the simple ratio calculated using the following formula:

$$\mathrm{BBvFr} = \frac{\text{Total Overstory Points with Intensity Values} \leq 50\,\mathrm{i} \text{ or} \geq 170\,\mathrm{i}}{\text{Total Overstory Points with Intensity Values} > 50\,\mathrm{i} \text{ and} < 170\,\mathrm{i}}. \quad (1)$$

The lower and upper intensity thresholds of 50 i and 170 i were found to be safe and consistent values for differentiating between BB and F intensity valued points based on inspection of the 40 randomly selected snag and 100 randomly selected live tree point clouds (Fig. 3).

2.4.2.2. Stage two — define BB and F intensity filtering thresholds. BBvFr was first used along with the maximum intensity value to automatically adjust the BB and F lower and upper intensity threshold values ($\mathrm{LInt_t}$ and $\mathrm{UInt_t}$) for each plot point cloud being analyzed. Through a manual process using the training datasets, the following linear equations and conditions were established to define the lower and upper BB and F intensity threshold values for each plot point cloud at both study locations:

$$\mathrm{LInt_t} = 20(\mathrm{BBvFr}) + 0.075(\mathrm{MaxInt}) + 26.5 \quad (2)$$

$$\mathrm{UInt_t} = 20(\mathrm{BBvFr}) + 0.1875(\mathrm{MaxInt}) + 100.25 \quad (3)$$

$$\begin{aligned} &\text{If } \mathrm{LInt_t} < 50,\ \mathrm{LInt_t} = 50\,\mathrm{i} \text{ If } \mathrm{LInt_t} > 70,\ \mathrm{LInt_t} = 70\,\mathrm{i} \\ &\text{If } \mathrm{UInt_t} < 150,\ \mathrm{UInt_t} = 150\,\mathrm{i} \text{ If } \mathrm{UInt_t} > 170,\ \mathrm{UInt_t} = 170\,\mathrm{i} \\ &\text{If Located in SF Area},\ \mathrm{LInt_t} = \mathrm{LInt_t} + 5\,\mathrm{i} \text{ If SF},\ \mathrm{UInt_t} = \mathrm{UInt_t} - 5\,\mathrm{i}. \end{aligned}$$

Of the two variables BBvFr has more influence on the threshold values, while maximum intensity provides minor adjustments. As BBvFr decreases the $\mathrm{LInt_t}$ increases and $\mathrm{UInt_t}$ decreases making the algorithm more sensitive to identifying snag points by allowing more points to be classified as BB and not F. Plots located in SF received a lower and upper intensity threshold correction of ± 5 i after all other conditions were applied. This correction helped reduce local intensity differences between the acquisitions (Fig. 5). The lower BB and F threshold values ranged from 50 i to 70 i at BMEF and 55 i to 75 i at SF, while the upper BB and F threshold values ranged from 150 i to 170 i at BMEF and 145 i to 165 i at SF.

2.4.2.3. Stage three — calculate neighborhood variable statistics. Once the BB and F intensity thresholds were calculated for each plot point cloud, they were used to calculate three neighborhood variable statistics for each point in the overstory. These statistics were then used in the conditional assessment stage to determine whether the individual lidar points were associated with a live tree or snag.

In theory, if a lidar point is associated with a live tree or snag then its neighboring points (i.e., points located within its local-area or neighborhood) are most likely to be associated with the same live tree or snag. Extending this theory, since snags are predominately comprised of BB intensity valued points, a point associated with a snag should have a higher concentration of BB intensity valued points located within its neighborhood compared to a point associated with a live tree. By analyzing the neighborhood BB concentration traits for each point, trends were identified and used to filter and classify each point as a live tree or snag point. Three neighborhood variables for each point were identified to be a robust combination for classifying the points: a sphere, a small cylinder and a large cylinder (Fig. 4).

All three neighborhood variables are created by forming a local-area centered on each point (Fig. 4). The sphere, created by forming a 1.5 m radius sphere around each point, provides information on a point's immediate vicinity. This variable is useful for identifying unique local attributes within tree crowns. The small cylinder, created by forming a 1 m radius cylinder around each point and projected only upward,

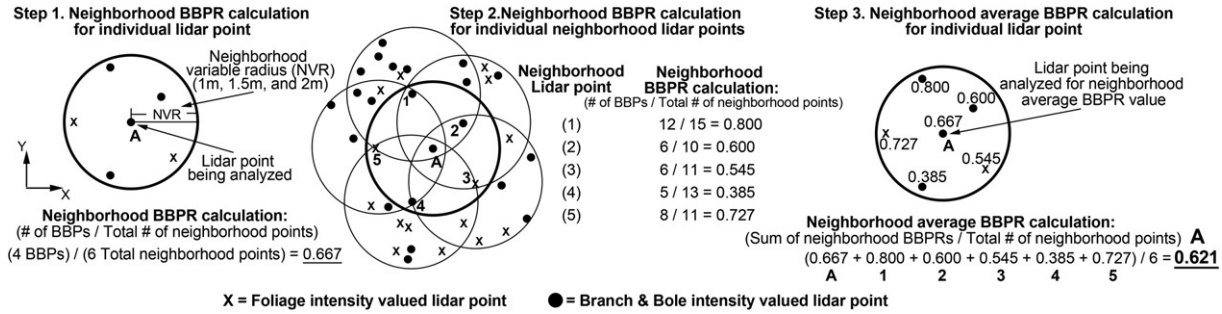

Fig. 6. Depiction of the three step process used to calculate the neighborhood average BBPR for each lidar point's three neighborhood variables (BBP = branch and bole intensity valued lidar point; BBPR = branch and bole lidar point ratio).

provides information about the vicinity located above and near each point. This variable is useful for identifying snag crowns protruding above live tree crowns. The large cylinder, created by forming a 2 m radius cylinder around each point and projected upward and downward, provides information about the general vicinity around each point. By providing more generalized 2D information, it is useful for determining the likelihood of a snag being located in the localized area.

Neighborhood average BB point ratios (BBPR) were calculated for each point's three neighborhood variables following the steps outlined in Fig. 6. Only overstory points were used in the calculations. The result was an average BBPR value ranging from 0 to 1 for each of the overstory point's three neighborhood variables. The closer the neighborhood average BBPR value is to 1, the higher the concentration of BB points in the point's neighborhood and the more likely it is to be associated with a snag. By using the neighborhood average BBPR value the local area of influence for each point is extended outside the individual point's neighborhood (Fig. 6 — step 2). This helps the algorithm gravitate to and identify the individual points most likely to be associated with a snag even within an individual snag's point cloud.

2.4.2.4. Stage four — identify individual snag points. Identification of individual snag points was completed by assessing each overstory point against a series of conditional assessments. The conditional assessments were based on two statistics from each of the three neighborhood variables: point density and average BBPR. In order for an individual point to be identified as a snag point it had to meet all the requirements for at least one conditional assessment. Four groups of conditional assessments were identified that accurately and robustly classified the overstory points in the diversity of natural conditions found at both study locations: 1) general, 2) small snag, 3) live crown edge, and 4) high canopy cover (Table 2). Each group targets a unique snag location scenario with some overlap between them. The 'general' group was the most robust group at identifying snag points in a broad range of situations. The 'small snag' group was created to find snag points associated with isolated snags that had lower point densities. The 'live crown edge' group was focused on finding snag points associated with snags located directly adjacent to and intermixing with live tree crowns. The 'high canopy cover' group was only used when the plot-level canopy cover was ≥55% to identify snag points associated with snags protruding above live canopy conditions.

Sensitivity of the conditional assessments is adjusted by shifting the neighborhood average BBPR value requirements. The magnitude of the shift (i.e., sensitivity level) is determined automatically using a decision tree based on BBvFr, canopy cover, and mean canopy height (Fig. 7). The objective of the decision tree is to adjust the sensitivity of the algorithm to match the intensity and stand conditions present in the area being assessed (i.e., windowed approach). The combination of these three variables provided the ability to classify local intensity and stand condition variation into logical groups. Sensitivity levels range from 0 to 5; a higher value is commensurate with more relaxed conditional assessment requirements. Fig. 8 provides an example of how the sensitivity

Table 2
The four groups of conditional assessments with their required neighborhood point density and average BBPR values (BBPR = branch and bole point ratio; PDR = point density requirement). Values are associated with an algorithm sensitivity level of 4.

Assessment group	Sphere		Small cylinder		Large cylinder	
	Point density (>=)	Average BBPR (>=)	Point density (>=)	Average BBPR (>=)	Point density (>=)	Average BBPR (>=)
General	PDR	0.99	–	0.99	–	0.70
	PDR	0.95	–	0.95	–	0.725
	PDR	0.90	–	0.90	–	0.75
	PDR	0.85	–	0.85	–	0.775
	PDR	0.80	–	0.80	–	0.80
Small snag	2 and (<=) PDR	0.95	2 and (<=) PDR	0.95	2 and (<=) PDR	0.60
	2 and (<=) PDR	0.90	2 and (<=) PDR	0.90	2 and (<=) PDR	0.65
	2 and (<=) PDR	0.85	2 and (<=) PDR	0.85	2 and (<=) PDR	0.75
Live crown edge	PDR	0.80	PDR	0.95	PDR*7	0.70
	PDR	0.85	PDR	0.90	PDR * 7	0.75
	PDR	0.90	PDR	0.85	PDR * 7	0.80
	PDR	0.95	PDR	0.80	PDR * 7	0.85
High canopy cover (only CC >= 55%)	PDR	0.95	PDR	0.95	PDR * 8	0.75
	…	…	…	…	…	
	PDR	0.95	PDR	0.95	PDR * 15	0.55
	PDR	0.90	PDR	0.90	PDR * 8	0.85
	…	…	…	…	…	…
	PDR	0.90	PDR	0.90	PDR * 15	0.65

PDR: Point density requirement based on plot-level point density (PLPD) defined classes.
(If PLPD <= 3, PDR = 3; if 3 < PLPD <= 6, PDR = 4; if 6 < PLPD <= 12, PDR = 5; if PLPD > 12, PDR = 8).

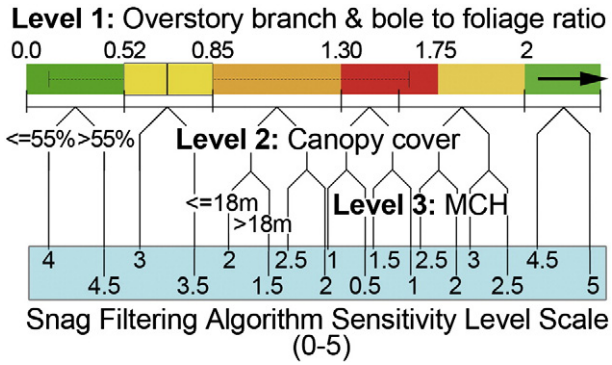

Fig. 7. Snag-filtering algorithm sensitivity decision tree used to determine the algorithm's conditional assessment values (MCH = mean canopy height).

value was used to adjust the general group conditional assessment requirements.

The neighborhood point density requirements used in the conditional assessments are automatically classified into four groups based on the plot-level point density (Table 2). They are used in two ways: 1) to insure there are enough neighborhood points within the sphere neighborhood variable to make the average BBPR value significant, and 2) to adjust the average large cylinder neighborhood BBPR value requirements (i.e., the higher the large cylinder neighborhood point density, the lower the requirement for large cylinder average BBPR). The point density requirements were not utilized in all conditional assessments.

2.4.2.5. Stage five — eliminate live tree points. After the individual snag point identification process was completed, all overstory points located within a 1 m radius cylinder of snag classified points were classified as snag points. Overstory points not receiving a snag classification were classified as live tree points and then eliminated from the overstory by replacing their height values with a zero value. The final result is a plot point cloud containing only snag classified points in the overstory and live tree points on the ground (i.e., zero height). The final step was to remove all understory points greater than 0.2 m in height. This

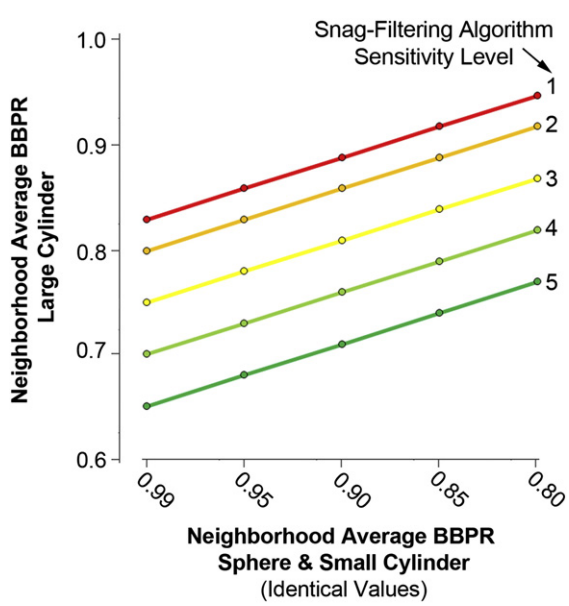

Fig. 8. Example of how the algorithm sensitivity value is used to adjust the 'General' conditional assessment group value requirements. Overstory lidar points with a large cylinder neighborhood average BBPR value above the appropriate line are classified as snag points (BBPR = branch and bole point ratio).

retains all points on or near the ground surface in the final point cloud, which is necessary to create an accurate canopy surface model in the next step.

The final individual snag-filtered plot point clouds from the training dataset were analyzed for accuracy and algorithm parameters were adjusted using a manual sequential process to develop the final algorithm definitions and parameters. Once the training of the snag-filtering algorithm was completed using the training dataset, it was applied to the independent plots (n = 153) to generate the final snag-filtered plot point clouds for analysis. These point clouds were then exported for use in the individual-tree segmentation procedure.

2.4.3. Individual-snag detection

Individual-snag detection was completed using a traditional airborne lidar individual-tree segmentation procedure (Kaartinen & Hyyppä, 2008; Vauhkonen et al., 2011). A canopy surface model was first created using the snag-filtered point cloud, and then individual-snags were located using an automated local-maxima detection algorithm to produce an individual-snag data file containing an ID, location (i.e., x- and y-UTM coordinates), and height value for each detected snag.

Canopy surface models can have various forms depending on how the surface is interpolated and smoothed, which all affect the ability to accurately identify individual trees. When the primary use for a canopy surface model is to detect individual-trees or snags, it is crucial the canopy surface model accurately represents individual trees or snags by providing a single height maxima for each tree while following crown profiles. In this study, the canopy surface models were created using the 'CanopyModel' command line utility processing program in the Fusion lidar software package (McGaughey, 2012). The following parameters and filters were used to create a canopy surface model that adequately characterized individual snags using the snag-filtered plot point clouds; a surface grid cell size of 0.85 m^2, application of both median and mean smoothing filters (5 × 5 grid cell windows), and preservation of local maxima using the 'peaks' switch within CanopyModel to force the surface to adhere to the tops of trees.

Individual snags were located from the canopy surface model by using the automated command line utility processing program 'CanopyMaxima' in the Fusion lidar software package (McGaughey, 2012). The program's default settings were used to locate individual-snags and export a tree list for each plot containing the x- and y-UTM coordinates and height values for each tree identified. The individual plot tree list files were combined and imported into ArcGIS for comparison and analysis. Trees located within the 5 m plot buffer areas were removed, resulting in the final lidar-derived plot-level snag stem map. The lidar-derived plot stem map was then compared to the field-derived plot stem map to determine snag detection and error rates.

2.4.4. Snag detection and error rates

Snag detection and error rates were generated by comparing the lidar- and field-derived stem maps in ArcGIS using the independent dataset. To determine if an individual snag was correctly detected, acceptable location distance errors had to be defined. Taking into account the positional accuracy of plot locations and the field methods used to locate individual trees, individual snag location errors were expected to be within ±1.5 m. This error only refers to the position at the base of the tree, without considering the potential deviations of a tree top relative to its base. Given the accuracy of the lidar acquisition (±15 cm) and the fact that the taller a snag is the more likely it is to have a greater deviation between its base and top locations, the thresholds for acceptable location distance errors were set as 3 m for snags <9 m in total height and 4.5 m for trees with total heights ≥9 m. If a lidar detected snag location was within the acceptable distance of a field measured snag, it was classified as detected. Only one field measured snag could be associated with each lidar detected snag location. Lidar detected snags not within the acceptable distance of any field measured snags

were classified as commission errors (i.e., a live tree or a portion of a live tree that was incorrectly classified as a snag). If a field measured snag was not detected using the lidar method it was classified as an omission error.

Snag detection rates are summarized for the three strata (i.e., BMEF, SF-ULS, and SF-MSHS) using various DBH and height criteria to help assess the method's accuracy and applicability in different forest types and stand conditions. Snag detection rate trends for lidar point density and canopy cover are presented to provide a better understanding of how these variables interact with the method. Lidar-derived and field-measured snag heights are compared using an ordinary least squares (OLS) regression analysis to determine if the method produced accurate height estimates.

Commission and omission errors are summarized categorically to provide insight on error causes and rates. Commission errors occurred when the lidar snag detection method falsely identified a live tree or a portion of a live tree as a snag. Individual commission errors were inspected and classified into one of the following seven categories: 1) dead top, 2) dead branches, 3) highest tree vigor risk rating, 4) high tree vigor risk rating with abnormal growth, 5) extreme snow bend, 6) multiple forks and crooks, and 7) stump sprouting black oak. Omission errors occurred when snags were not detected using the lidar snag detection method. The reasons for these errors were explored and classified into the following six categories: 1) sharing space with live trees, 2) low point density, 3) too many foliage valued intensity points, 4) dead foliage still attached, 5) canopy surface model, and 6) stump sprouting black oak.

3. Results

3.1. Snag detection rates

Snag DBH distributions and detection rates for the three strata using various DBH and height criteria scenarios are summarized in Fig. 9. The three strata produced similar snag detection rates that increased as the size of the snags increased. The strata combined detection rate for snags in smaller DBH classes (12–50 cm) was 42.5% (±2.7%) using the ≥3 m minimum height criteria; and 61.3% (±4.7%) for larger DBH classes (50–90+ cm). Detection rates were also calculated for different ≥DBH scenarios (i.e., number of snags over a specified DBH). The strata combined detection rate for snags with a minimum height of 3 m and DBHs ≥ 25 cm was 56.0% (±2.9%), increasing to 75.0% (±12.5%) for DBHs ≥ 90 cm. On average, detection rates increased by 0.4% for every 1 cm DBH increase and 1.9% for every 1 m increase in height. The overall detection rates for the various DBH scenarios increased by an average of 5.9% for every 3 m increase in the height criteria, with the largest average increases occurring between the ≥3 and 6 m height criteria (6.3%).

For BMEF, the majority of snags were smaller with DBHs < 37 cm (Fig. 9). The overall detection rate for these snags was 40.0% (±4.4%) using the 3 m minimum height criteria; while the detection rate for snags with DBH ≥ 37 cm was much higher at 56.1% (±7.8%). Detection rates for the ≥DBH class scenarios followed a similar pattern for all three height criteria, steadily increasing to the ≥50 cm DBH class and then leveling off for the higher ≥DBH classes. The detection rates for the various DBH scenarios increased by an average of 7.6% for every 3 m increase in the minimum height criteria.

For SF-ULS, the snag DBH distribution was similar to BMEF, with a majority of snags having DBHs < 37 cm (59%). The detection rate for snags with DBHs < 37 cm using the 3 m minimum height criteria was 37.7% (±5.8%), and 51% (±7.1%) for snags with DBHs ≥ 37 cm. Overall, the detection rates were the lowest compared to the other two strata and remained relatively stable for the various DBH scenarios (Fig. 9). For the three minimum height criteria scenarios (i.e., 3, 6, and 9 m), the detection rate increased at the lowest average rate (1.1%) as ≥DBH class criteria increased. The detection rates for the various DBH scenarios did however display the highest average increase for every 3 m increase in the minimum height criteria at 10.6%.

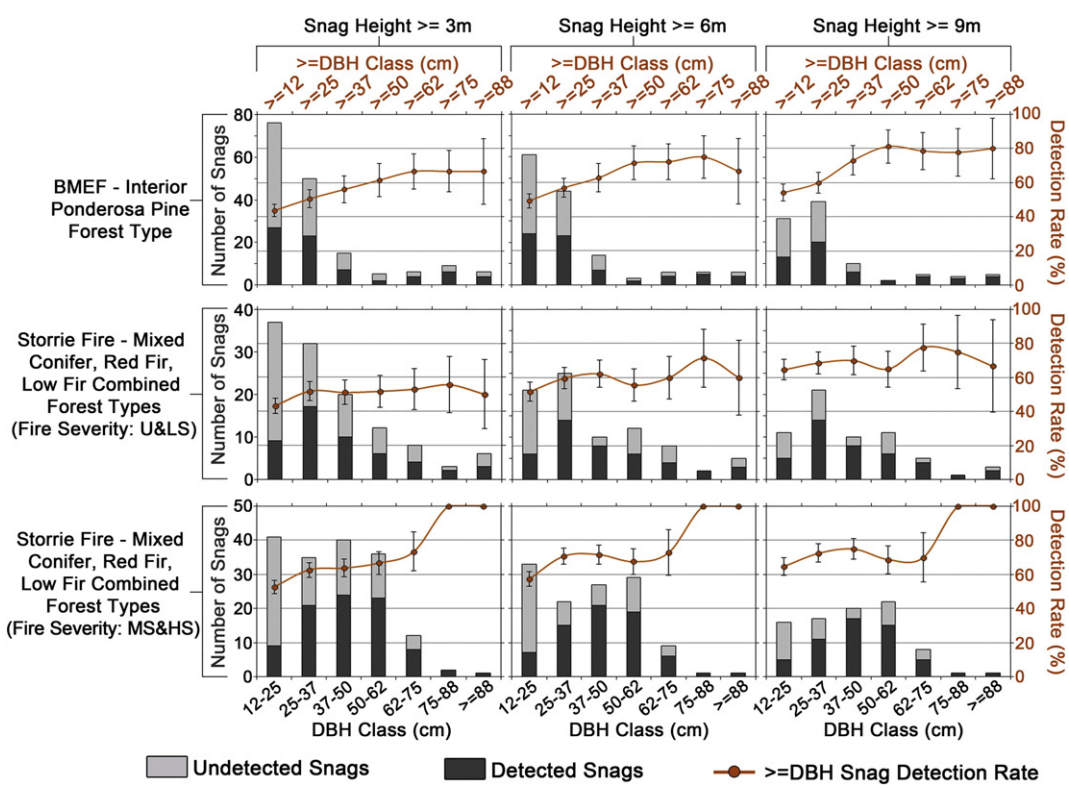

Fig. 9. Snag diameter distribution and detection rate summaries for the three strata under various DBH and height scenarios. ≥DBH class detection rates are defined as all snags with DBHs greater than or equal to the DBH listed (i.e., ≥25 DBH class = detection rate for all trees with DBHs ≥ 25 cm).

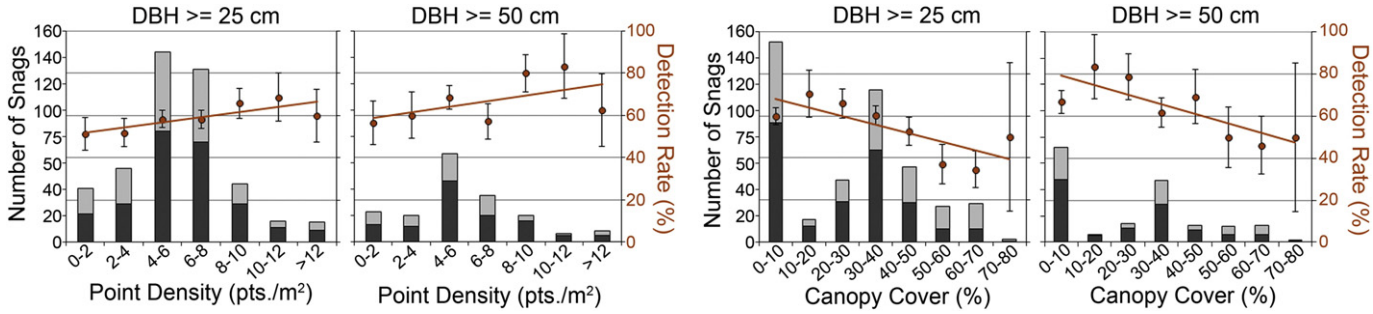

Fig. 10. Lidar point density and canopy cover detection rate trends for two different ≥DBH class scenarios (DBH ≥ 25 cm and 50 cm). Black and gray bars represent the proportion of detected and undetected snags respectively for the individual point density and canopy cover classes.

For SF-MSHS, the snag DBH distribution was relatively uniform for snags <62 cm DBH and decreased significantly for snags ≥62 cm DBH. The overall detection rates were the highest for this stratum, with a majority of the rates between 60 and 80%. Detection rates for the ≥DBH class scenarios followed a similar pattern for all three height criteria, slowly increasing to the ≥62 cm DBH class and then increasing to 100% for the higher ≥DBH classes. The 100% detection rates for snags with DBHs ≥ 75 cm were based on low snag sample sizes (n ≤ 4) and should be viewed with caution. The stratum also had the lowest average rate of increase (2.5%) between the three minimum height criteria scenarios.

3.2. Snag detection rate trends

Lidar point density and canopy cover both exhibited trends that affected the method detection performance (Fig. 10). Detection rates tended to increase as point densities increased and decrease as canopy cover increased. Both trends remained stable as snag size increased. The point density trend was not as significant as the canopy cover trend, with an average trend slope of 0.026 for point density versus an average trend slope of −0.043 for canopy cover.

3.3. Snag heights

Overall the lidar-derived heights displayed a good relationship with the field-measured heights, explaining a large amount of the variation associated with field-measured heights from the linear regression model ($R^2 = 0.87$). The lidar-derived snag heights exhibited a small negative bias that became less prevalent as the height increased (Fig. 11). The height bias was −0.89 m for snags with field-measured heights ≤25 m, and −0.22 m for snags with heights >25 m. The residual standard error for the OLS model was ±3.14 m, with a median error of −0.66 m.

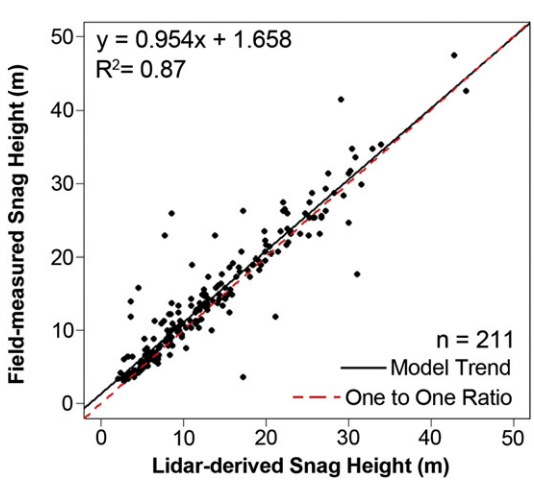

Fig. 11. Lidar-derived snag heights versus field-measured snag heights.

3.4. Commission errors

Commission error rates varied for the three strata (Table 3). BMEF had the lowest commission rate (0.96 ha^{-1}), followed by SF-ULS (3.20 ha^{-1}) and SF-MSHS (6.42 ha^{-1}). Commission errors were most often associated with smaller trees, with 56% of them having DBHs ≤ 25 cm and 81% of them having DBHs ≤ 50 cm. SF-MSHS had 12 commission errors that were associated with 6 stump sprouting black oak trees. If these errors are removed from the commission error assessment, the SF-MSHS stratum had the lowest commission error rate (0.49 ha^{-1}).

The causes of the commission errors varied, but were most often associated with stump sprouting black oak trees that maintained dead crowns (38%) and live trees containing a high percentage (≥90%) of dead crown on at least one side of the tree crown (25%) (Table 4). All commission errors associated with trees with DBHs ≥ 50 cm (n = 6) were associated with having either a large dead top that comprised ≥25% of the tree crown, a tree vigor risk rating at the highest level (i.e., death imminent), or a high tree vigor risk rating with an abnormal growth pattern (e.g., witches broom, severe crooks or sweeps). Two commission errors were caused by smaller trees (DBH ≤ 25 cm) exhibiting extreme snow bend (≥45°), and one error was caused by a tree exhibiting abnormal growth patterns with multiple forks and crooks.

3.5. Omission errors

The proportion of undetected snags for each of the six error causation categories is presented in Table 5. Over half of the omission errors (56.3%) were caused by snags that shared space with at least one live tree. These situations made it difficult to identify the individual snag

Table 3
Summary of commission error rates for the three strata by DBH class (BMEF = Blacks Mtn. Exp. Forest; SF-ULS = Storrie Fire unchanged and low fire severity; SF-MSHS = Storrie Fire medium and high fire severity).

DBH class (cm)	BMEF	Storrie Fire (ULS)	Storrie Fire (MSHS)	Total (DBH class)	Storrie Fire (MSHS w/out black oak)
12–25	34	2	12	18	–
25–37	2	3	–	5	–
37–50	2	–	1	3	1
50–62	1	–	–	1	–
62–75	1	–	–	1	–
75–88	2	1	–	3	–
>=88	–	1	–	1	–
Total (strata)	12	7	13	32	1
Commission error rate (ha^{-1})	0.96	3.20	6.42	1.92	0.49

Table 4
Summary of commission error causes by DBH class.

DBH class (cm)	Dead top (>=25% of canopy)	Dead branches (one side (>=25%) of canopy dead)	Highest risk rating tree[a]	High risk rating tree[b] (w/ abnormal growth characteristic)	Extreme snow bend or lean	Multiple forks and crooks	Stump sprouting black oak (w/ dead canopy)
12–25	–	3	–	1	2	–	12
25–37	–	3	1	–	–	1	–
37–50	–	2	1	–	–	–	–
50–62	1	–	–	–	–	–	–
62–75	–	–	–	1	–	–	–
75–88	1	–	1	1	–	–	–
>=88	–	–	1	–	–	–	–
Total (32)	2	8	4	3	2	1	12

Abnormal growth characteristics include witches broom, crooks and sweeps.
[a] The highest risk rating trees display signs of imminent death; such as sparse crowns with necrotic foliage, multiple dead branches and no new growth.
[b] High risk rating trees display unhealthy crowns and indications of low vigor, thinning crowns with dead branches and limited growth.

points because the neighborhood average BBPR statistics associated with the snag points received more influence from the neighboring live tree points with intensity values in the foliage range. The next highest omission error cause was associated with low point densities (17.2%). Snags with low point densities were typically smaller and were often not identified using the method because they did not meet the required point density threshold conditions used in the snag-filtering algorithm. Snags containing too many foliage valued intensity points caused 11.4% of the omission errors. Snags with dead foliage still attached caused 4.6% of the errors. Dead attached foliage returned intensity values in the foliage intensity range, therefore this category could also be grouped with the 'higher percentage of foliage valued intensity points' category. The canopy surface model creation method caused 8.6% of the omission errors by smoothing neighboring snag canopy surfaces together into one canopy surface with one local-maxima. Black oak trees with complex crowns caused the lowest percentage of omission errors (2.0%).

4. Discussion

4.1. Snag detection

The method presented in this study was able to accurately detect and locate a large proportion of snags in all strata with low commission error rates. Snag detection rates increased as the size of snags increased (i.e., DBH and height). Most forest management snag stocking guidelines and standards are focused on larger snags, as they provide more wildlife habitat potential. For the areas in this study, a common snag size threshold used in stocking guidelines is DBH ≥ 37 cm. The method presented in this paper provided an overall combined detection rate of 58.5% (±3.7%) for snags meeting this size threshold based on the independent dataset.

The three strata provided an opportunity to explore the method's performance in various forest types and stand conditions. The BMEF and SF-ULS strata demonstrated how the method performs in more natural forest stand conditions for these forest types. Both strata had similar overall detection rates (BMEF: 43.7%; SF: 43.2%), but the detection rates at BMEF increased at a much higher rate as snag DBH increased. This is most likely associated with the more dense and complex stand structures found in the SF forest types (i.e., MC, LF and HF) compared to the BMEF forest type (i.e., interior ponderosa pine). There was a larger sample size at BMEF in a broader range of natural stand conditions. Thus, more weight should be given to the results at BMEF. In natural stand conditions for the forest types analyzed in this study, detection rates will likely be between 40 and 60% for smaller snags (DBH < 37 cm, heights ≥ 3 m), and 55–80% for larger snags (DBH ≥ 37 cm, heights ≥ 3 m).

As expected, most of the snags at SF were located in the SF-MSHS stratum (60% with 27% less area sampled). This stratum had very low canopy covers (0–25%) and live tree densities (0–20%), which resulted in higher detection rates than would be expected in natural forest conditions. The SF-MSHS stratum detection rates were consistently higher than 65% for DBHs ≥ 37 cm snags, which demonstrates the ability of the method to successfully detect individual snags post-wildfire (~9 years) in medium and high fire severity areas. This suggests that this method could provide utility for live versus dead tree assessments following wildfire and other disturbance events.

4.2. Factors affecting snag detection

Snag detection rates using this method were affected by a number of uncontrollable and controllable factors. Uncontrollable factors were associated with forest stand and individual snag characteristics, while controllable factors were associated with the quality of the lidar data and the individual-snag detection methods.

4.2.1. Uncontrollable factors

Uncontrollable factors associated with forest stand characteristics included canopy cover and snag location with respect to live trees. Canopy cover is an uncontrollable factor that significantly affected the methods' ability to detect snags (Fig. 10). As canopy cover increases the likelihood of snags intermixing with live tree crowns also increases, making snag points more difficult to identify with the snag-detection algorithm.

Six uncontrollable individual snag characteristics were identified that adversely affected individual snag detection. First, snags with dead foliage attached often had a large proportion of their lidar points classified as having foliage intensity values, which caused them to be classified as live tree points during the snag-filtering algorithm. Overcoming this problem will be difficult using discrete-return lidar data, even with better intensity calibration. This also highlights a temporal component associated with snag detection using this method; as time since death passes, snag detection will increase as the amount of dead foliage and fine branches decrease. In the example of a large-scale disturbance, such as wildfire or insect outbreak, acquisition of lidar data for snag detection using this or similar methods should be timed in

Table 5
Proportion of undetected snags by causation categories.

	Sharing space with live tree(s)	Low lidar point density	Too many foliage intensity points	Dead foliage still attached	Canopy surface model	Black oak complex crown	Total undetected (n)
Proportion of undetected snags (%)	56.3 (2.5)	17.2 (1.9)	11.4 (1.6)	4.6 (1.1)	8.6 (1.4)	2.0 (0.7)	396

consideration of needle- or leaf-cast. In this same context, in areas with coniferous and deciduous trees intermixing, snag detection will likely be improved if the lidar data acquisition is completed in leaf-on conditions as it was in this study.

The second individual tree characteristic found to affect detection rates was associated with black oak, a deciduous tree species found infrequently the MC forest type. All black oak snags sampled in this study were located on four plots in the SF-MSHS stratum. The growth characteristics associated with these trees produced a unique situation which affected omission errors when they were a snag (i.e., no live stump sprouting present) and commission errors when they exhibited live foliage in the form of stump sprouting. In all cases, these trees were associated with multiple stems generating from one unique base. Due to the sampling protocol each unique stem with a DBH ≥ 11.5 cm was treated as a separate snag. Making matters even more troublesome was the fact that they do not follow a simple vertical growth pattern. They typically grow with spread out dome-shaped crowns. This either caused the canopy surface model associated with these trees to generate too many or not enough local maxima, which in turn caused the commission and omission errors respectively. If black oak trees were removed from the analysis, the overall detection and error rates would improve.

The next three individual tree characteristics that affected the ability to detect individual snags were associated with trees declining in vigor, having abnormal growth patterns (e.g. crooks, sweeps, crotches), or having dead tops. Many of the commission errors were caused by live trees exhibiting one of these conditions. Even though these trees often caused commission errors, they also highlight the ability of the method to identify live trees displaying unique characteristics often related to tree health or vigor. Trees with these characteristics often provide valuable wildlife habitat (Bull, Parks, & Torgersen, 1997), so there may be an opportunity to use lidar for identifying these habitat features as well.

The last individual tree characteristic found to affect detection rates was associated with snow bent trees (i.e., trees with snow bend angle ≥45°). These trees have boles that are more exposed to airborne lidar scanning which resulted in a higher density of BB intensity valued points within the neighborhood variables. On two occasions these trees were classified as snags. There were a total of 12 snow bent trees (bending ≥ 45°) located on the sampled plots, so the error rate was relatively low (16.7%).

4.2.2. Controllable factors

Controllable factors affecting the ability of the method to detect snags can be partitioned into three categories: 1) lidar acquisition and intensity calibration, 2) snag-filtering algorithm, and 3) individual-snag detection methods. Adjustments to these can either improve or deteriorate the snag detection rates.

Lidar acquisition parameters and intensity variability play a significant role in the usefulness of lidar data. Both lidar acquisitions in this study were collected by the same vendor, which reduced the variability between the lidar datasets. The vendor also used the automatic variable gain setting during acquisition in both study areas. In forested environments, the automatic variable gain setting remains relatively stable due to the homogenous nature of these environments (i.e., low variability in the target population surface reflectance and composition). This aids with the usefulness of the intensity information by reducing the variable gain settings' influence on intensity variability. In environments where target populations have more surface reflectance and composition variability (e.g., urban areas) the usefulness of the un-calibrated intensity information will likely be reduced. Post-acquisition intensity calibration was not completed for the lidar data in this study. At the time of this study, post-acquisition intensity calibration techniques are being developed and are becoming more available. Most calibration routines are based on the assessment of the acquisition parameters against reference settings that are then used to normalize intensity values. These normalized intensity values should provide more useful information for lidar filtering and analysis.

Sufficient lidar point densities are required for the filtering algorithm to successfully identify individual snag points. Based on the lidar point density trends found in this study (Fig. 10), a point density of ≥4 first and single return points m^{-2} should provide an adequate amount of data to successfully detect a majority of large snags. Higher point densities should improve results. Identifying the optimal lidar point density for snag detection will vary depending on the quality of the intensity information, forest stand characteristics (e.g., forest type, tree density, and crown structure), and snag-filtering algorithm parameters.

The snag-filtering algorithm displayed encouraging potential in its ability to identify individual snag points. The average BBPR value for each of the three neighborhood variables can be thought of as the probability of each point being associated with either BB or F. In this context, the higher the sum of the three neighborhood average BBPR values is for each point (maximum of 3), the more likely that point is associated with a snag. Expanding on this application, the neighborhood average BBPR values could have additional uses for assessing tree vigor or health indices, since trees with lower vigor typically have lower proportions of foliage compared to trees with higher vigor. The neighborhood average BBPR values might also be useful for species identification, especially when differentiating between deciduous and coniferous species. It's also important to note that the snag-filtering algorithm used in this application was created and then tested on independent datasets that came from the same lidar acquisitions. While modifications made to the snag-filtering algorithm between the two lidar acquisition datasets were relatively minor, more testing of the filtering algorithm with additional lidar datasets is necessary to understand the variation and sensitivity associated with the method.

Neighborhood attribute point cloud filtering displayed promising utility as a new lidar analysis technique for accurately classifying overstory lidar points to either a live tree or snag. The primary objective of neighborhood attribute point based filtering is to create an automated method to identify and accurately assign the proper forest attribute to each lidar point, or to assign individual forest attribute probabilities or weights to each lidar point. This additional analysis step should provide an enhanced lidar analysis framework for both plot-based and individual forest attribute assessments since lidar points not associated with the forest attribute(s) of interest can either be removed or given less influence. As an example in the context of a live-tree variable plot-based lidar assessment (e.g., basal area and volume), the combined local-variable BBPR values could be used to assign live tree vs. dead tree weights to each overstory point. These weights could then be used to create lidar point cloud explanatory variables that more accurately represent the live-tree variable of interest (i.e., dead tree points are either removed or provide less influence). There a vast array of filtering techniques and methods that can be explored for assigning lidar points to forest attributes of interest using the inherent information provided by lidar. This was the first attempt at using neighborhood attribute point cloud filtering to differentiate between live and dead tree lidar points, thus it is likely there are ways to improve the filtering methods in this study. New airborne remote sensing systems that integrate multiple sensors in various spectrums onto one platform with lidar data (e.g., G-LiHT (Cook et al., 2013)) would likely increase our ability to filter and classify lidar data.

The individual-snag detection procedure was able to correctly identify and locate a majority of snags in all strata. Having live tree points removed from the point clouds used to create the canopy surface model made it easier to identify individual snag canopies. Even with the respectable results, the canopy surface model creation method still had two downfalls. First, snags located directly adjacent to each other were sometimes reduced to one snag canopy during canopy surface model creation. This could be overcome by using a smaller grid cell size during creation of the canopy surface model; however this would likely result in higher commission error rates. Second, in areas where deciduous trees intermix with coniferous species the canopy surface model will likely have problems characterizing one or the other. A method that

treats them separately might help, but this would be more difficult to implement.

The individual-tree segmentation method provided relatively accurate height estimates with a small negative bias. Negative biases have been found in many lidar studies for tree heights, although they are typically larger than the one found in this study (Gatziolis, Fried, & Monleon, 2010; Stereńczak & Zasada, 2011). It is hypothesized that the snag-filtering algorithm, particularly the last snag point identification step where neighboring points located within a 1 m cylinder of the classified snag points were also classified as snag points, caused the negative bias to be smaller than expected by occasionally including neighboring tree points that were located above the snag which resulted in the heights being overestimated. These height overestimation errors offset a portion of the negative bias; therefore if they were removed the negative bias would be higher. The negative bias was likely a function of the physical characteristics associated with snags (e.g., smaller target surface area at the top for decayed snags). Higher point densities would likely help reduce the height bias, or a bias correction factor could be applied.

4.3. Applications

The application of the method to different airborne lidar datasets, forest types and stand structures warrants further investigation to better understand the variation and sensitivity of the method. The snag-filtering algorithm parameters will likely need to be tuned for each lidar dataset and forest type (e.g., neighborhood sizes, BB and F intensity thresholds, and point density and BBPR condition requirements), which can be accomplished using a training dataset. Training datasets should be comprised of as many plots as possible, while maintaining a sufficient independent dataset. This study randomly selected ~25% of the plots to use as the training dataset. In the future as more datasets are analyzed, it could become possible to standardize the filtering algorithm parameters for various lidar acquisitions and forest type attributes.

Applications of the method could help overcome a number of the problems associated with the ability to estimate and monitor snags. The method provides the ability to estimate snag densities for various size classes, while also providing the spatial distribution of individual snags. Both the applications should help increase our understanding of snag dynamics in forest ecosystems, and enhance our ability to develop and assess snag stocking standards. Proper determination of individual snag detection rates and snag density estimates currently requires accurate field-derived stem map data. However, if average detection rates along with commission and omission errors are known for various forest types and lidar parameters, it could become possible to estimate snag densities using only airborne lidar data in the future.

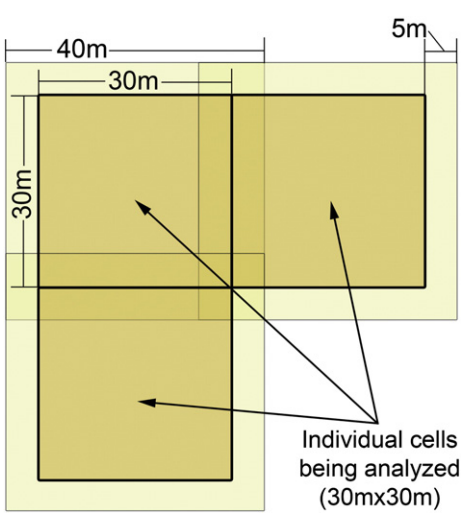

Fig. 12. Depiction of the iterative area segmentation procedure used to apply the snag-filtering algorithm to lidar datasets. The individual areas without their 5 m buffers are aggregated back together after the filtering algorithm is applied.

Application of the snag-filtering algorithm across entire lidar datasets can be accomplished using a sequential procedure, where the filtering algorithm is applied to individually segmented areas ranging from 0.01 to 0.2 ha in size that are aggregated back together after the filtering algorithm is applied (Fig. 12). Since the snag-filtering algorithm requires multiple loops through the lidar points being analyzed, the size of the grid cells, the point density, and the forest overstory characteristics within each grid cell will determine the efficiency of the algorithm. For this study the plot size was ~0.081 ha with a 5 m buffer, the snag-filtering algorithm's run time averaged 2.24 s with a range from 0.68 to 11.06 s. Expanding the average value to a 100 ha area, the filtering algorithm would be completed in ~46 min with similar lidar point densities and forest overstory characteristics.

5. Conclusions

This study presented a new method for identifying and locating individual snags across forested landscapes using airborne lidar data. The method introduced a new lidar analysis technique; neighborhood attribute point-based filtering focused on accurately assigning the proper forest attribute to each lidar point. The neighborhood attribute point-based filtering technique in this study used the location along with the intensity and density attributes associated with the individual points to identify whether overstory lidar points were associated with live or dead trees. The snag-filtered point clouds were then used to identify individual snags. This was the first attempt to filter lidar data with this purpose, so it is expected that improvements to the filtering methods are available. Even without improvement, the method presented was able to identify a large proportion snags and a majority of the larger snags in natural stand conditions with very low commission error rates. Stands with high mortality (i.e., post-disturbance — medium and high wildfire severity) produced even better results. The method is automated and efficient once the filtering algorithm is trained and provides the ability to obtain snag density estimates and an accurate snag stem map for the majority of larger snags. Additional benefits are produced by the snag-filtered lidar data that should provide and enhanced lidar analysis framework for modeling live and dead tree variables. Given the difficulties associated with the estimation of snags across the landscape, the method presented could provide a more robust and accurate alternative where airborne lidar data are available. The method warrants further investigation with additional lidar datasets in various forest types and conditions to better understand the sensitivity and variability associated with the method.

Acknowledgments

This study was conducted in collaboration with the U.S. Forest Service, Lassen National Forest. The authors gratefully acknowledge the reviewer's comments and contributions that greatly improved the manuscript; the field work and additional help of Thomas Fisher, David McClung and Travis Springer; and the quality input given by Mike Simpson, Leo Yanez, and Joesph Bowles from the U.S. Forest Service — Deschutes National Forest.

References

Anderson, H. -E., Clarkin, T., Winterberger, K., & Strunk, J. (2009). An accuracy assessment of positions obtained using survey- and recreation-grade global positioning system receivers across a range of forest conditions within Tanana valley on Interior Alaska. *Western Journal of Applied Forestry*, *24*(3), 128–136.

Bate, L.J. (1995). *Monitoring woodpecker abundance and habitat in the central Oregon Cascades.* Moscow, ID: University of Idaho, 116 (M.S. thesis).

Bate, L.J., Garton, E.O., & Wisdom, M.J. (1999). *Estimating snag and large tree densities and distributions on a landscape for wildlife management.* USDA Forest Service General Technical Report PNW-GTR-425. US: Pacific Northwest Research Station, Portland, OR.

Bater, C.W., Coops, N.C., Gergel, S.E., LeMay, V., & Collins, D. (2009). Estimation of standing dead tree class distributions in northwest coastal forests using lidar remote sensing. *Canadian Journal of Forest Resources*, *39*, 1080–1091.

Boddy, L., Frankland, J.C., & van West, P. (2008). *Ecology of saprotrophic basidiomycetes.* Amsterdam: Elsevier, 386.

Boyd, D.S., & Hill, R.A. (2007). *Validation of airborne lidar intensity values from a forested landscape using Hymap data: Preliminary analysis.* IAPRS*XXXVI, Part 3/W52*, .

Bull, E.L., Holthausen, R.S., & Marx, D.B. (1990). How to determine snag density. *Western Journal of Applied Forestry*, *5*(2), 56–58.

Bull, E.L., Parks, C.G., & Torgersen, T.R. (1997). *Trees and logs important to wildlife in the interior Columbia River basin.* USDA Forest Service General Technical Report PNW-GTR-391. US: Pacific Northwest Research Station, Portland, OR.

Bütler, R., & Schlaepfer, R. (2004). Spruce snag quantification by coupling colour infrared aerial photos and a GIS. *Forest Ecology and Management*, *195*, 325–339.

Cook, B.C., Lawrence, A., Nelson, R.F., Middleton, E.M., Morton, D.C., McCorkel, J.T., et al. (2013). NASA Goddard's LiDAR, hyperspectral and thermal (g-LiHT) airborne imager. *Remote Sensing*, *5*, 4045–4066.

Croft, F.C., Heller, R.C., & Hamilton, D.A. (1982). *How to interpret tree mortality on large-scale color aerial photographs.* USDA Forest Service General Technical Report INT-GTR-124. US: Intermountain Forest and Range Experiment Station, Ogden, UT.

Crotteau, J.S., Varner, J.M., III, & Ritchie, M.W. (2012). Post-fire regeneration across a fire severity gradient in the southern Cascades. *Forest Ecology and Management*, *287*, 103–112.

Donoghue, D.N.M., Watt, P.J., Cox, N.J., & Wilson, J. (2007). Remote sensing of species mixtures in conifer plantations using Lidar height and intensity data. *Remote Sensing of Environment*, *110*(4), 509–522.

Ducey, M.J., Jordan, G.J., Gove, J.H., & Valentine, H.T. (2002). A practical modification of horizontal line sampling for snag and cavity tree inventory. *Canadian Journal of Forest Research*, *32*, 1217–1224.

Eyre, F.H. (1980). Forest cover types of the United States and Canada. Washington, DC: Society of American Foresters.

Fan, Z., Shifley, S.R., Thompson, F.R., & Larsen, D.R. (2004). Simulated cavity tree dynamics under alternative timber harvest regimes. *Forest Ecology and Management*, *193*, 399–412.

Ferrell, G.T. (1989). *Ten-year risk-rating systems for California red fir and white fir: Development and use.* USDA Forest Service General Technical Report PSW-GTR-115. US: Pacific Southwest Research Station, Berkeley, CA.

Franklin, J.F., Berg, D.R., Thornburgh, D.A., & Tappeiner, J.C. (1997). Alternative silvicultural approaches to timber harvesting: Variable retention harvest systems. In K.A. Kohm, & J.F. Franklin (Eds.), *Creating a forestry for the 21st century: The science of ecosystem management* (pp. 67–98). Washington, D.C.: Island Press.

Frescino, T.S., Edwards, T.C., & Moisen, G.G. (2001). Modeling spatially explicit forest structural attributes using generalized additive models. *Journal of Vegetation Science*, *12*, 15–26.

Gatziolis, D., Fried, J.S., & Monleon, V.S. (2010). Challenges to estimating tree height via LiDAR in closed-canopy forest: A parable from Western Oregon. *Forest Science*, *56*(2), 139–155.

Gray, A. (2003). Monitoring stand structure in mature coastal Douglas-fir forests: Effect of plot size. *Forest Ecology and Management*, *175*, 1–16.

Guo, Q., Kelly, M., Gong, P., & Liu, D. (2007). An object-based classification approach in mapping tree mortality using high spatial resolution imagery. *GIScience & Remote Sensing*, *44*, 24–47.

Haara, A., & Nevalainen, S. (2002). Detection of dead or defoliated spruces using digital aerial data. *Forest Ecology and Management*, *160*, 97–107.

Hamilton, R., Megown, K., Ellenwood, J., Lachowski, H., & Maus, P. (2010). *Advances in threat assessment and their application to forest and rangeland management.* USDA Forest Service General Technical Report PNW-GTR-802. US: Pacific Northwest Research Station, Portland, OR.

Harmon, M.E. (2002). *Moving towards a new paradigm for woody detritus management.* USDA Forest Service General Technical Report PNW-GTR-181. US: Pacific Northwest Research Station, Portland, OR.

Harmon, M.E., & Sexton, J. (1996). Guidelines for measurements of woody detritus in forest ecosystems. *Publication No. 20* (pp. 73). Seattle, WA: U.S. Long-Term Ecological Research (LTER) Network Office, University of Washington.

Hawbaker, T.J., Keuler, N.S., Lesak, A.A., Gobakken, T., Contrucci, K., & Radeloff, V.C. (2009). Improved estimates of forest vegetation structure and biomass with a Lidar-optimized sampling design. *Journal of Geophysical Research*, *114*. http://dx.doi.org/10.1029/2008JG000870 G00E04.

Holloway, G.L., Caspersen, J.P., Vanderwel, M.C., & Naylor, B.J. (2007). Cavity tree occurrence in hardwood forests of central Ontario. *Forest Ecology and Management*, *239*(1–3), 191–199.

Holmgren, J., & Persson, Å. (2004). Identifying species of individual trees using airborne laser scanning. *Remote Sensing of Environment*, *90*, 415–423.

Hudak, A.T., Crookston, N.L., Evans, J.S., Falkowski, M.J., Smith, A.M.S., Gessler, P.E., et al. (2006). Regression modeling and mapping of coniferous forest basal area and tree density from discrete-return lidar and multispectral satellite data. *Canadian Journal of Remote Sensing*, *32*, 126–138.

Jonsson, B.G., Kruys, N., & Ranius, T. (2005). Ecology of species living on dead wood — Lessons for dead wood management. *Silva Fennica*, *39*, 289–309.

Kaartinen, H., & Hyyppä, J. (2008). EuroSDR/ISPRS Commission II project: "Tree Extraction" — final report. *Official publication no. 53. EuroSDR* (pp. 60). Germany: Frankfurt am Main.

Kelly, M., Shaari, D., Guo, Q., & Liu, D. (2004). A comparison of standard and hybrid classifier methods for mapping hardwood mortality in areas affected by "sudden oak death". *Photogrammetric Engineering and Remote Sensing*, *70*(11), 1229–1239.

Kenning, R., Ducey, M., Brisette, J., & Gove, J. (2005). Field efficiency and bias of snag inventory methods. *Canadian Journal of Forest Research*, *35*(12), 2900–2910.

Kim, Y., Yang, Z., Cohen, W.B., Pflugmacher, D., Lauver, C.L., & Vankat, J.L. (2009). Distinguishing between live and dead standing tree biomass on the North Rim of Grand Canyon National Park, USA using small-footprint lidar data. *Remote Sensing of Environment*, *113*, 2499–2510.

Krebs, C.J. (1989). Ecological methodology. New York: Harper Collins Publishers, Inc.

Lämas, T., & Stahl, G. (1998). On the accuracy of line transect sampling of rare forest objects. In P. Bachmann, M. Ko¨hl, & R. Pa¨ivinen (Eds.), *Assessment of biodiversity for improved forest planning* (pp. 273–281). Dordrecht: Kluwer Academic Publishers.

Laudenslayer, W.F., Jr. (2002). *Cavity-nesting bird use of snags in eastside pine forests of northeastern California.* USDA Forest Service General Technical Report PSW-GTR-181. U.S. Pacific Southwest Research Station, Fresno, CA.

Leckie, D.G., Jays, C., Gougeon, F.A., Sturrock, R.N., & Paradine, D. (2004). Detection and assessment of trees with *Phellinus weirii* (laminated root rot) using high resolution multi-spectral imagery. *International Journal of Remote Sensing*, *25*(4), 793–818.

Lefsky, M.A., Cohen, W.B., Harding, D.J., & Parker, G.G. (2002). Lidar remote sensing for forest ecosystem studies. *BioScience*, *52*, 19–30.

Lim, K., Treitz, P., Baldwin, K., Morrison, I., & Green, J. (2003). Lidar remote sensing of biophysical properties of tolerant northern hardwood forests. *Canadian Journal of Remote Sensing*, *29*, 648–678.

Maltamo, M., Eerikäinen, K., Pitkänen, J., Hyyppä, J., & Vehmas, M. (2004). Estimation of timber volume and stem density based on scanning laser altimetry and expected tree size distribution functions. *Remote Sensing of Environment*, *90*(3), 319–330.

Maltamo, M., Malinen, J., Packalén, P., Suvanto, A., & Kangas, J. (2006). Nonparametric estimation of stem volume using airborne laser scanning, airborne photography, and stand-register data. *Canadian Journal of Forest Research*, *36*(2), 426–436.

Martinuzzi, S., Vierling, L.A., Gould, W.A., Falkowski, M.J., Evans, J.S., Hudak, A.T., et al. (2009). Mapping snags and understory shrubs for a Lidar-based assessment of wildlife habitat suitability. *Remote Sensing of Environment*, *113*, 2522–2546.

McGaughey, R.J. (2012). *FUSION/LDV: Software for LiDAR data analysis and visualization — V3.10.* USDA Forest Service. US: Pacific Northwest Research Station, Portland, OR, 168.

Mehtätalo, L. (2006). Eliminating the effect of overlapping crowns from aerial inventory estimates. *Canadian Journal of Forest Research*, *36*(7), 1649–1660.

Mellen, K., Marcot, B.G., Ohmann, J.L., Waddell, K., Livingston, S.A., Willhite, E.A., et al. (2006). *DecAID, the decayed wood advisor for managing snags, partially dead trees, and down wood for biodiversity in forests of Washington and Oregon. Version 2.0.* Portland, OR: USDA Forest Service, Pacific Northwest Region and Pacific Northwest Research Station; USDI Fish and Wildlife Service, Oregon State Office.

Miller, J.D., Knapp, E.E., Key, C.H., Skinner, C.N., Isbell, C.J., Creasy, R.M., et al. (2008). Calibration and validation of the relative differenced Normalized Burn Ratio (RdNBR) to three measures of fire severity in the Sierra Nevada and Klamath Mountains, California, USA. *Remote Sensing of Environment*, *113*, 645–656.

Morsdorf, F., Mårell, A., Koetz, B., Cassagne, N., Pimont, F., Rigolot, E., et al. (2010). Discrimination of vegetation strata in a multi-layered Mediterranean forest ecosystem using height and intensity information derived from airborne laser scanning. *Remote Sensing of Environment*, *114*, 1404–1415.

Næsset, E. (2002). Predicting forest stand characteristics with airborne scanning laser using a practical two-stage procedure and field data. *Remote Sensing of Environment*, *80*, 88–99.

Oliver, W.W. (2000). *Ecological research at Blacks Mountain Experimental Forest in northeastern California.* USDA Forest Service General Technical, Report. Albany, Calif: Pacific Southwest Research Station (PSW-GTR-179).

Pasher, J., & King, D.J. (2009). Mapping dead wood distribution in a temperate hardwood forest using high resolution airborne imagery. *Forest Ecology and Management*, *258*, 1536–1548.

Pesonen, A., Maltamo, M., Eerikäinen, K., & Packalén, P. (2008). Airborne laser scanning based prediction of coarse woody debris volumes in a conservation area. *Forest Ecology and Management*, *255*, 3288–3296.

Reitberger, J., Schörr, C.L., Krzystek, P., & Stilla, U. (2009). 3D segmentation of single trees exploiting full waveform LIDAR data. *Journal of Photogrammetry and Remote Sensing*, *64*, 561–574.

Reutebuch, S.E., Andersen, H. -E., & McGaughey, R.J. (2005). Light detection and ranging (LIDAR): An emerging tool for multiple resource inventory. *Journal of Forestry*, *103*(6), 286–292.

Ritchie, M.W., Skinner, C.N., & Hamilton, T.A. (2007). Probability of wildfire-induced tree mortality in an interior pine forest: Effects of thinning and prescribed fire. *Forest Ecology & Management*, *247*, 200–208.

Rose, C.L., Marcot, B.G., Mellen, T.K., Ohmann, J.L., Waddell, K.L., Lindley, D.L., et al. (2001). Decaying wood in Pacific Northwest forests: Concepts and tools for habitat management. In D.H. Johnson, & T.A. O'Neil (Eds.), *Wildlife-habitat*.

Salman, K.A., & Bongberg, J.W. (1942). Logging high risk trees to control insects in the pine stands of northeastern California. *Journal of Forestry*, *40*(7), 533–539.

Stereńczak, K., & Zasada, M. (2011). Accuracy of tree height estimation based on LIDAR data analysis. *Folia Forestalia Polonica, Series A*, *53*(2), 123–129.

Thomas, J.W., Anderson, R.G., Maser, C., & Bull, E.L. (1979). Wildlife habitats in managed forests; the Blue Mountains of Oregon and Washington. *USDA Forest Service Ag. Handbook No. 553* (pp. 512).

Vauhkonen, J., Ene, L., Gupta, S., Heinzel, J., Holmgren, J., Pitkänen, J., et al. (2011). Comparative testing of single-tree detection algorithms under different types of forest. *Forestry, International Journal of Forest Research*. http://dx.doi.org/10.1093/forestry/cpr051.

Wang, Y., Weinacker, H., Koch, B., & Sterenczak, K. (2008). LIDAR point cloud based fully automatic 3D single tree modelling in forest and evaluations of the procedure. *International Archives of Photogrammetry, Remote Sensing and Spatial Information Sciences, 37 (Part B6b)*. (pp. 45–51).

Wing, B.M., Ritchie, M.W., Boston, K., Cohen, W.B., Gitelman, A., & Olsen, M.J. (2012). Prediction of understory vegetation cover with airborne lidar in an interior ponderosa pine forest. *Remote Sensing of Environment*, *124*, 730–741.

Yoccoz, N.G., Nichols, J.D., & Boulinier, T. (2001). Monitoring of biological diversity in space and time. *Trends in Ecology and Evolution*, *16*(8), 446–453.